



22 **Abstract**

23 Marine phytoplankton are responsible for about half of the photosynthesis on Earth. Many are  
24 mixotrophs, combining photosynthesis with heterotrophic assimilation of organic carbon but the  
25 relative contribution of these two carbon sources is not well quantified. Here, single-cell  
26 measurements reveal that *Prochlorococcus* at the base of the photic zone in the Eastern  
27 Mediterranean Sea are obtaining only ~20% of carbon required for growth by photosynthesis.  
28 Consistently, laboratory-calibrated evaluations of *Prochlorococcus* photosynthesis indicate that  
29 carbon fixation is systematically too low to support published *in situ* growth rates in the deep  
30 photic layer of the Pacific Ocean. Furthermore, agent-based model simulations show that  
31 mixotrophic cells maintain realistic growth rates and populations 10s of meters deeper than  
32 obligate photo-autotrophs, deepening the nutricline and Deep Chlorophyll Maximum by ~20 m.  
33 Time-series of *Prochlorococcus* ecotype-abundance from the subtropical North Atlantic and North  
34 Pacific suggest that up to 30% of the *Prochlorococcus* cells live where light intensity is not enough  
35 to sustain obligate photo-autotrophic populations during warm, stratified periods. Together,  
36 these data and models suggest that mixotrophy underpins the ecological success of a large  
37 fraction of the global *Prochlorococcus* population and its collective genetic diversity.

38

39

40 Photosynthesis by phytoplankton provides most of the energy and fixed carbon that support  
41 marine food webs and carbon reservoirs<sup>1</sup>. However, few phytoplankton are strictly photo-  
42 autotrophic<sup>2</sup>. Many phytoplankton also utilize dissolved organic matter, taking up particulate  
43 detrital organic matter or preying upon other living cells and even harvesting organelles<sup>2</sup>.  
44 Mixotrophic lifestyles, in which cells both fix carbon and use exogenously available organic  
45 carbon, may enhance fitness when the relative availability of inorganic resources differs from  
46 physiological demands<sup>3</sup>. This may occur, for example, where light intensity is low but inorganic  
47 nutrients are abundant. Despite the potential importance of mixotrophy to phytoplankton life  
48 history, the contribution of heterotrophic carbon assimilation to phytoplankton growth is not well  
49 quantified<sup>4</sup>. Simulations suggest that mixotrophy may be a globally significant carbon source for  
50 phytoplankton<sup>5</sup> but this prediction is currently difficult to quantitatively test with empirical data.  
51 One reason is that dissolved organic carbon (DOC) in the oceans constitutes an extremely complex  
52 mixture of compounds<sup>6,7</sup>, most of which are uncharacterized. This means that uptake  
53 measurements using specific organic carbon sources (e.g. glucose, amino acids)<sup>8,9</sup> do not  
54 represent the entirely available DOC pool and may underestimate the actual DOC uptake rates,  
55 and hence mixotrophy of major phytoplankton species<sup>10</sup>.

56 *Prochlorococcus* are the most abundant phototrophic cells on Earth, actively growing at depths  
57 ranging from the ocean surface down to the base of the photic zone (~160 m)<sup>11</sup>. Across these  
58 depths, photosynthetically available radiation (PAR) varies over 3-4 orders of magnitude, a  
59 challenge which the diverse *Prochlorococcus* lineage faces using a variety of adaptations in their  
60 photosynthetic apparatus<sup>11,12</sup>. These adaptations have led to the diversification of  
61 *Prochlorococcus* into high-light and low-light adapted clades<sup>11,12</sup>. In addition, *Prochlorococcus* are  
62 mixotrophs, able to uptake dissolved organic compounds such as glucose<sup>8</sup>, pyruvate<sup>13</sup>, amino  
63 acids<sup>9</sup>, nucleotides<sup>10</sup> and perhaps DMSP<sup>14,15</sup>. Yet, to what extent DOC uptake can supplement or  
64 replace photosynthetically fixed carbon for respiration and/or growth in this globally-abundant  
65 lineage is still unknown<sup>10</sup>. Available evidence suggests that while mixotrophy helps  
66 *Prochlorococcus* survive limited periods of darkness, axenic cells die after ~1 week if not exposed  
67 to light<sup>13,16</sup> indicating that light harvesting, and possibly photosynthesis, are likely obligate.

68 Here, we take a multi-faceted approach to evaluate the contribution of heterotrophic carbon  
69 assimilation to *Prochlorococcus* in the oceans. We first use isotopic measurements to quantify  
70 photosynthesis and N uptakes in wild *Prochlorococcus* populations at the base of the photic zone

71 in the Mediterranean Sea. Then we compare observed growth rates from the Pacific Ocean with  
72 purely photo-autotrophic growth rates simulated by a laboratory-calibrated photo-physiological  
73 model. We also use an individual-based model to illustrate how mixotrophy provides a fitness  
74 advantage and deepens the nutricline. Finally, we use time-series observations of vertical profiles  
75 of *Prochlorococcus* ecotypes in subtropical gyres to show that several clades rely extensively on  
76 mixotrophic carbon assimilation. Overall, these results suggest that up to a quarter of depth  
77 integrated carbon assimilation by *Prochlorococcus* originates from DOC, with implications for  
78 global C cycles, and that mixotrophy is essential to support a significant fraction of  
79 *Prochlorococcus* diversity.

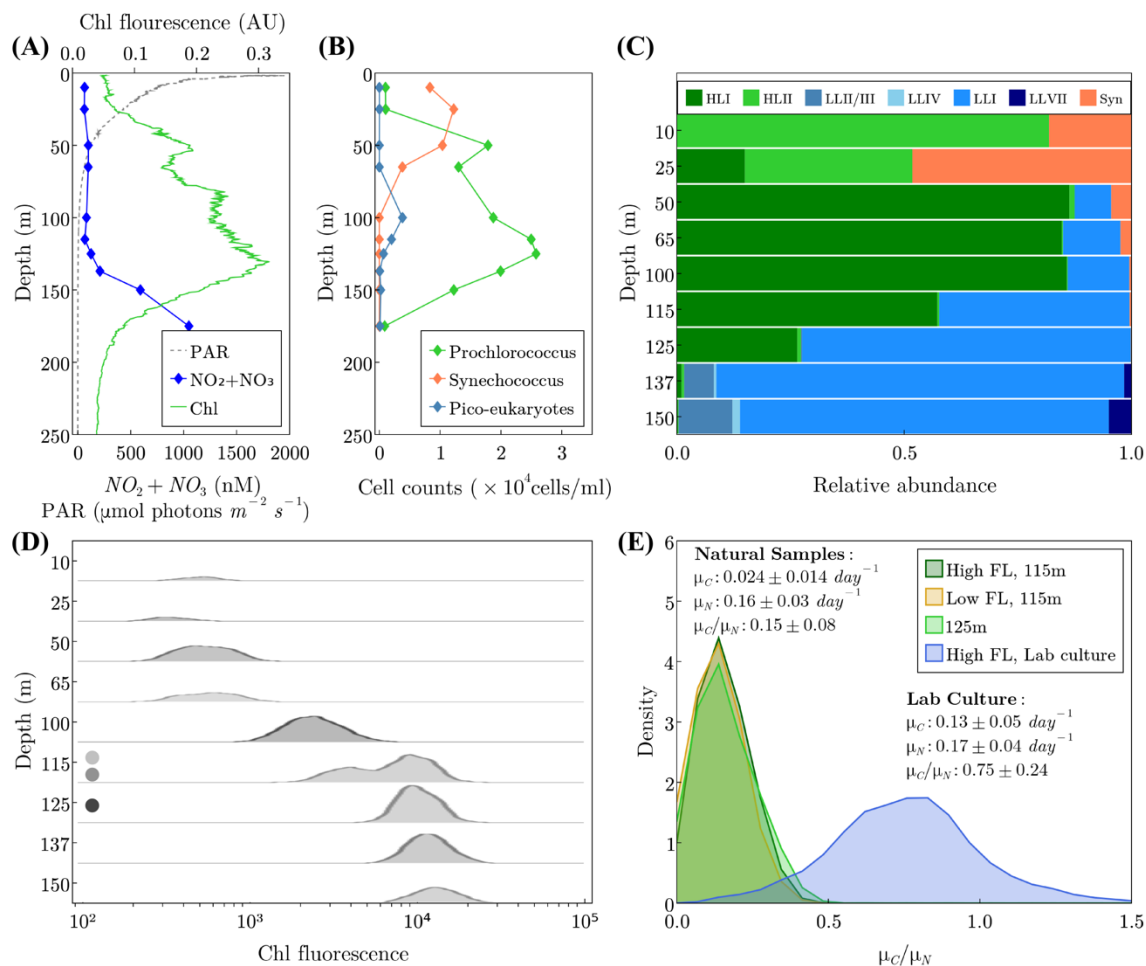
80

## 81 **Results and discussion**

### 82 *Carbon and nitrogen uptake in wild samples from the base of the photic zone.*

83 To evaluate the relative contributions of photosynthesis and heterotrophic carbon uptake in a  
84 natural *Prochlorococcus* population from the base of the photic zone, where light may be limiting,  
85 we assess the *Prochlorococcus* population structure and per-cell activity during late summer in  
86 the ultra-oligotrophic Eastern Mediterranean Sea<sup>17</sup>. At the time of sampling, the water column  
87 was highly stratified, nutrients were depleted down to around 140 m, and a prominent Deep  
88 Chlorophyll Maximum (DCM) was observed at depth of ~115 m (Figure 1A). *Prochlorococcus* were  
89 the numerically dominant phytoplankton below the surface (Fig 1B), and could be divided into  
90 two populations based on the per-cell fluorescence – a low fluorescence population from the  
91 surface to 115 m and a high fluorescence population from 115-150 m, with an overlap at 115 m  
92 (Figure 1C, D). The shift in the per-cell chlorophyll fluorescence in *Prochlorococcus* with depth is  
93 commonly observed<sup>18–20</sup>, and is usually attributed to a change in the genetic composition of the  
94 population, from High-Light adapted cells (HL, low fluorescence) to Low-Light adapted (LL, high  
95 fluorescence) ones<sup>19</sup>. However, phenotypic heterogeneity (acclimation) can also contribute to this  
96 phenomenon<sup>21</sup>, and indeed amplicon sequencing of the Internal Transcribed Spacer between the  
97 16S and 23S genes (ITS)<sup>21,22</sup> revealed a gradual transition from HL to LL clades around the DCM,  
98 suggesting both genotypic and phenotypic shifts with depth (Figure 1C). The flow cytometry and  
99 genetic data are both consistent with previous studies<sup>21,23</sup>, and suggest that the water column had  
100 been relatively stable for at least 3-4 days prior to sampling<sup>20</sup>. Notably, the light intensity at the

101 DCM ( $\sim 3\text{-}5 \mu\text{mol photons m}^{-2} \text{s}^{-1}$  during the afternoon, Figure 1A) is potentially enough under  
 102 laboratory conditions to support the growth of some LL strains but not sufficient for active growth  
 103 of most HL strains<sup>24</sup>. Since HL cells comprise >50% of the *Prochlorococcus* population at 115 m  
 104 and about 25% at 125 m, this suggests that a significant fraction of the *Prochlorococcus* cells in  
 105 these samples are living under conditions where photosynthesis cannot support growth (Figure  
 106 1C).



107

108 **Figure 1: Nutrient uptake of naturally occurring *Prochlorococcus* populations at the Eastern**  
 109 **Mediterranean Sea.** (A) Depth profiles of Photosynthetically Available Radiation (PAR),  $\text{NO}_2 + \text{NO}_3$   
 110 and Chlorophyll. (B) Phytoplankton cell counts using flow cytometry. (C) Relative abundance of  
 111 different *Prochlorococcus* clades across the water column, determined by ITS sequencing. Note  
 112 the change in Chl fluorescence without a concomitant change in population structure between 60  
 113 to 100 m, as well as the presence of LL clades above 115 m and HL clades at 125 m. (D) Density

114 plots of *Prochlorococcus* per-cell chlorophyll fluorescence. Note the double population at 115 m.  
115 The circles represent the populations sorted and analyzed by nanoSIMS. (E) Density plots of the  
116 ratios of C-specific C uptake rate ( $\mu_C$ ) to N-specific N uptake rate ( $\mu_N$ ) from NanoSIMS analysis of  
117 each sorted sub-population from 115 m, the single population from 125 m, and lab cultures. The  
118 numbers of cells measured in each population are 45 (LL 115m), 49 (HL 115m), 55 (125m), and  
119 489 (lab culture).

120

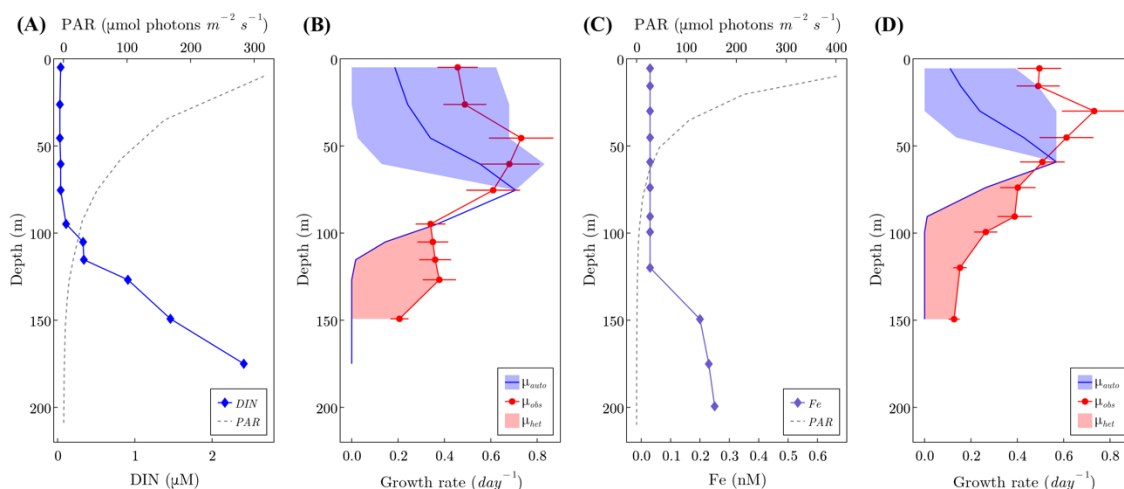
121 We next measured the uptake of  $^{13}\text{C}$ -labelled bicarbonate (representing C-fixation through  
122 photosynthesis) and of  $^{15}\text{N}$ -labeled ammonium (representing nitrogen uptake) in single  
123 *Prochlorococcus* cells from the DCM, using Nanoscale Secondary Ion Mass Spectrometry  
124 (NanoSIMS). Essentially all of the *Prochlorococcus* cells at 115 and 125 m depth were active  
125 (photosynthesized and took up  $\text{NH}_4$ ). The observation that essentially all of the *Prochlorococcus*  
126 cells in natural samples are active is consistent with a similar study in the North Pacific<sup>25</sup>, and  
127 suggests that dead or chlorotic cells observed in laboratory cultures<sup>13,26</sup> may be relatively rare in  
128 nature, at least during midday at the DCM. Nevertheless, the per-cell photosynthesis rates at  
129 these depths were not sufficient to support the growth rates indicated by the nitrogen-specific  
130 nitrogen uptake rates, even though the uptake experiments were performed when light intensity  
131 was maximal (Figure 1E). Previous studies from multiple oceanic regions based on cell cycle  
132 analysis and on  $^{14}\text{C}$  incorporation into divinyl-chlorophyll indicate that *Prochlorococcus* cells at  
133 depths of 100-150 m replicate every 4-7 days (a growth rate of  $0.14\text{-}0.25 \text{ day}^{-1}$ )<sup>27-30</sup>. However,  
134 the observed C-specific C uptake rate ( $\mu_C$ ) was only  $\sim 0.024 \text{ day}^{-1}$ , too low to support these  
135 expected growth rates, while the observed N-specific N uptake rate ( $\mu_N$ ) was  $\sim 0.16 \text{ day}^{-1}$   
136 indicating a doubling time of  $\sim 6$  days. Furthermore,  $\mu_C/\mu_N$  was only  $\sim 0.15$  in the field, much lower  
137 than normal cells which are expected to be  $\sim 1$  ( $\mu_C \approx \mu_N$ ). Indeed,  $\mu_C/\mu_N$  in lab cultured  
138 *Prochlorococcus* was  $\sim 0.75$  (Figure 1E). Taken together, these quantitative observations suggest  
139 that  $>80\%$  of the C required for the expected growth rate of these *Prochlorococcus* cells at the  
140 DCM must come from non-photosynthetic sources.

141

142 *Evaluation of potential growth rate profiles.*

143 Our Mediterranean samples suggest that a large fraction of carbon assimilated by *Prochlorococcus*  
144 in the deeper reaches of the photic zone is of organic origin. By comparing measured profiles of  
145 growth rates and modeling photosynthetic carbon fixation from sites in the Pacific, we ask if this  
146 is consistent in other regions and infers the water column integrated contribution of  
147 heterotrophy. Vaultot et al.<sup>31</sup> and Liu et al.<sup>32</sup> reported vertical profiles of *Prochlorococcus* division  
148 rates based on cell-cycle analysis in the Equatorial Pacific (EqPac, 0°N, 140°W) and North Pacific  
149 Subtropical Gyre (HOT, 22°45'N, 158°W; Station ALOHA), respectively. These data were obtained  
150 in the context of an extensive biogeochemical survey (JGOFS EqPac)<sup>33</sup> and time-series station  
151 (HOT)<sup>34</sup> and are associated with rich contextual data sets including observations of cell counts,  
152 photon fluxes and nutrient concentrations (Figure 2A, C). Calibrated by observed, noon-time PAR  
153 profiles, we simulated the daily cycle of photosynthesis and the vertical profiles of  
154 *Prochlorococcus*' carbon-specific, net photosynthesis rate ( $day^{-1}$ ). We simulated both HL and LL  
155 ecotypes, using laboratory calibrations of the photosynthesis-irradiance relationship from Moore  
156 and Chisholm<sup>24</sup>. Similarly, using allometric scaling for fixed-nitrogen, phosphate and dissolved iron  
157 uptake rates<sup>35,36</sup>, along with observed environmental concentrations, we evaluated the nutrient-  
158 specific uptake rates ( $day^{-1}$ ). Full details are presented in Materials and Methods. The estimated,  
159 purely autotrophic growth rates were determined by the most limiting resource at each depth  
160 (Figure 2B, D). Light and carbon fixation strongly limited the simulated autotrophic growth in the  
161 deeper region of the photic layer, while fixed nitrogen (HOT), iron (EqPac) and carbon fixation,  
162 due to photo-inhibition, were important near the surface (Figure 2). While the observed growth  
163 rates at the surface were mostly within the ranges predicted from the photophysiological  
164 parameters of HL and LL strains (blue shade in Figure 2B and D), the model failed to resolve the  
165 observed growth rates below ~75-100 m at both stations. Rather, the model unequivocally  
166 suggests that photosynthesis alone cannot account for the observed division rates at depth. We  
167 interpret the differences between the modeled autotrophic and observed actual growth rates at  
168 depth (red shading) to infer the minimal rate of organic carbon assimilation of *Prochlorococcus*.  
169 The two stations represent very different physical and biogeochemical regimes, yet show similar  
170 qualitative structure. Mixotrophy appears to become significant at different depths at the two  
171 stations (95 m at HOT and 60 m at EqPac) but at similar level of PAR ( $\sim 15 \mu mol photons m^{-2} s^{-1}$ ,  
172  $\sim 5\%$  of surface PAR). Using observed cell densities<sup>31,32</sup> and assumed cellular carbon quotas<sup>37</sup> we  
173 estimated the vertically integrated autotrophic net primary production for *Prochlorococcus* to be  
174  $\sim 0.35 gC m^{-2} day^{-1}$  at HOT and  $\sim 0.20 gC m^{-2} day^{-1}$  at EqPac, with vertically integrated

175 heterotrophic contributions (based on the red shading in Figures 2B and D) of  $\sim 0.075$   
 176  $gC\ m^{-2}\ day^{-1}$  at HOT and  $\sim 0.069\ gC\ m^{-2}\ day^{-1}$  at EqPac. In other words, assimilation of  
 177 organic carbon is inferred to support  $\sim 18\%$  of total *Prochlorococcus* biomass production at HOT  
 178 and  $\sim 25\%$  at EqPac. Furthermore, organic carbon uptake contributes  $\sim 80\%$  at HOT and  $54\%$  at  
 179 EqPac of the total production below the depth where the contribution of mixotrophy is greater  
 180 than photosynthesis, broadly consistent with the isotopic inference from the deep photic zone in  
 181 the Mediterranean. We note that this model does not take into account exudation of organic  
 182 carbon by *Prochlorococcus* which is not well constrained experimentally and would likely reduce  
 183 the inferred growth rates at the surface<sup>38-41</sup>. Indeed, mixotrophy (uptake of glucose and amino  
 184 acids) has been observed in surface *Prochlorococcus*<sup>9,10</sup>, suggesting that our estimate provides a  
 185 lower bound of the contribution of mixotrophy to integrated *Prochlorococcus* production.



186

187 **Figure 2. Simulated growth rates at HOT and EqPac.** (A), (C) Observations of PAR and dissolved  
 188 inorganic nitrogen (DIN) at the Hawaii Ocean Time-series (HOT, panel A) and of PAR and dissolved  
 189 iron (Fe) at the equatorial Pacific (EqPac, panel C). (B), (D) Simulated autotrophic growth rate  
 190 (blue line) and observed growth rates (red line with dots, data from<sup>42</sup>) at HOT (B) and EqPac (D).  
 191 The blue shade represents the difference between simulated HL and LL ecotypes, and the red  
 192 shade represents the inferred heterotrophic growth rate. A 19% error of observed growth rate is  
 193 included both at HOT and EqPac according to Vaultot et al.<sup>31</sup>.

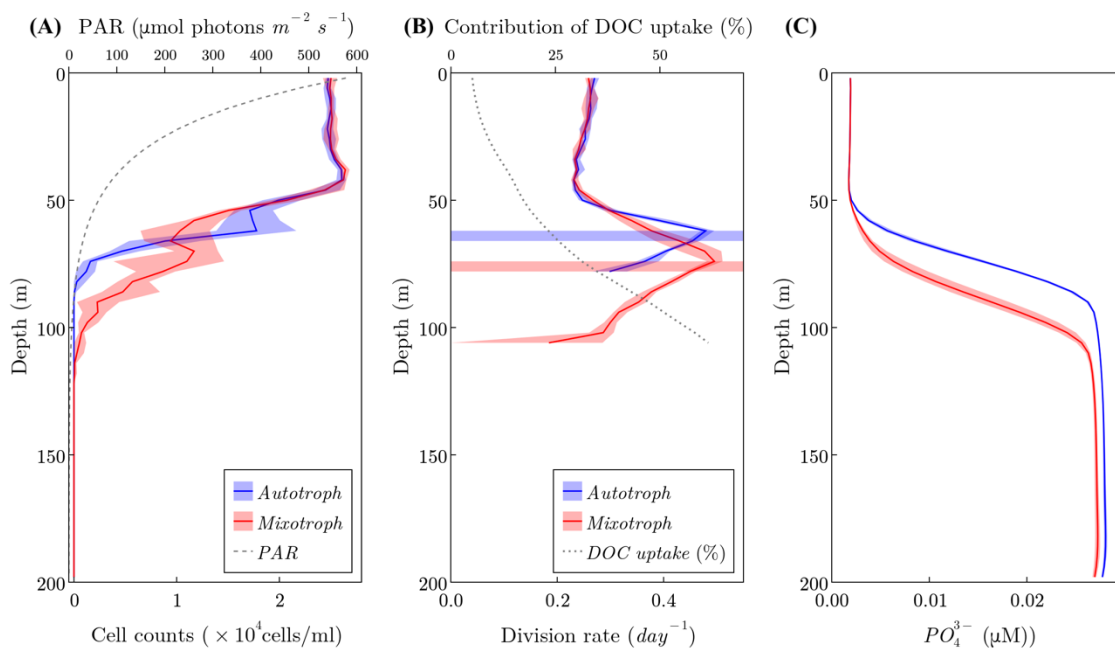
194

195 *Simulations in a dynamic water column.*



196 To investigate the implications of mixotrophy on biogeochemical dynamics, we employed an  
197 individual-based modeling approach (see Method for details), simulating trajectories of individual  
198 *Prochlorococcus* cells (or super-agents representing many cells) through light and nutrient  
199 environments in a two-dimensional, highly resolved turbulent fluid flow (see supporting movie).  
200 Inorganic nutrients and a DOC-like tracer are represented by density-based equations. Briefly,  
201 individuals fix carbon by photosynthesis and take up inorganic nitrogen and phosphorus. Two  
202 idealized types of individuals are simulated separately, one with a strict photo-autotrophic  
203 lifestyle and the other which is mixotrophic and able to assimilate carbon from the DOC-like  
204 substance. The mixotrophic individual cannot live strictly heterotrophically, as suggested by Coe  
205 et al.<sup>13</sup>, which we parameterize as requiring 1% of the incorporated C to come from  
206 photosynthesis. In Figure 3A we illustrate horizontally-averaged profiles of cell density from the  
207 purely autotrophic and mixotrophic simulations, illustrating how mixotrophy supports a  
208 population of *Prochlorococcus* below ~75 m. The simulated daily division rate of  $\sim 0.2 \text{ day}^{-1}$  at  
209 depth (Figure 3B) is consistent with the published cell-cycle profiles from the subtropical and the  
210 Equatorial Pacific<sup>31,32</sup> and is a bit higher than the aforementioned inferred division rate in the  
211 Mediterranean based on  $\text{NH}_4$  uptake. Mixotrophs and autotrophs share the same division rate  
212 ( $\sim 0.3 \text{ day}^{-1}$ ) in the mixed layer (surface 50 m) where the inorganic nutrient is the limiting factor  
213 in the simulations. The autotrophs then reach a maximum daily division rate of  $\sim 0.5 \text{ day}^{-1}$  at 60  
214 m depth where the transition of N to C limitation happens, and then decrease rapidly to zero at  
215 90 m depth due to light limitation. In contrast, the mixotrophs have a deeper maximum growth  
216 rate of  $\sim 0.5 \text{ day}^{-1}$  at 80 m depth where the transition of N to C limitation occurs and gradually  
217 decrease to  $\sim 0.2 \text{ day}^{-1}$  at 125 m depth (Figure 3B). The deeper maximum division depth of the  
218 mixotrophs and their ability to maintain a population at depths where photosynthesis is not  
219 sufficient are supported by the DOC utilization, which is presented as a black line in Figure 3B. In  
220 the mixotrophic simulation, the contribution of DOC uptake to the vertically integrated total  
221 production is ~12%; ~43% when light becomes the limiting factor, below the red stripe in Figure  
222 3B. The contribution of DOC and the maximal depth at which *Prochlorococcus* can grow are  
223 broadly consistent with the division rate profile model and are sensitive to parameter values  
224 which control the nutritional value of the DOC-like substance (and which cannot be *a priori*  
225 constrained by empirical data at this point; see Materials and Methods). Notably, the horizontal  
226 stripes in Figure 3B indicate the depth at which limitation shifted from nutrients to C in the two

227 ensembles of simulations. This horizon is deeper when the cells are mixotrophic and leads to a  
 228 significantly deeper nutricline in the simulation with mixotrophic cells (Figure 3C).



229

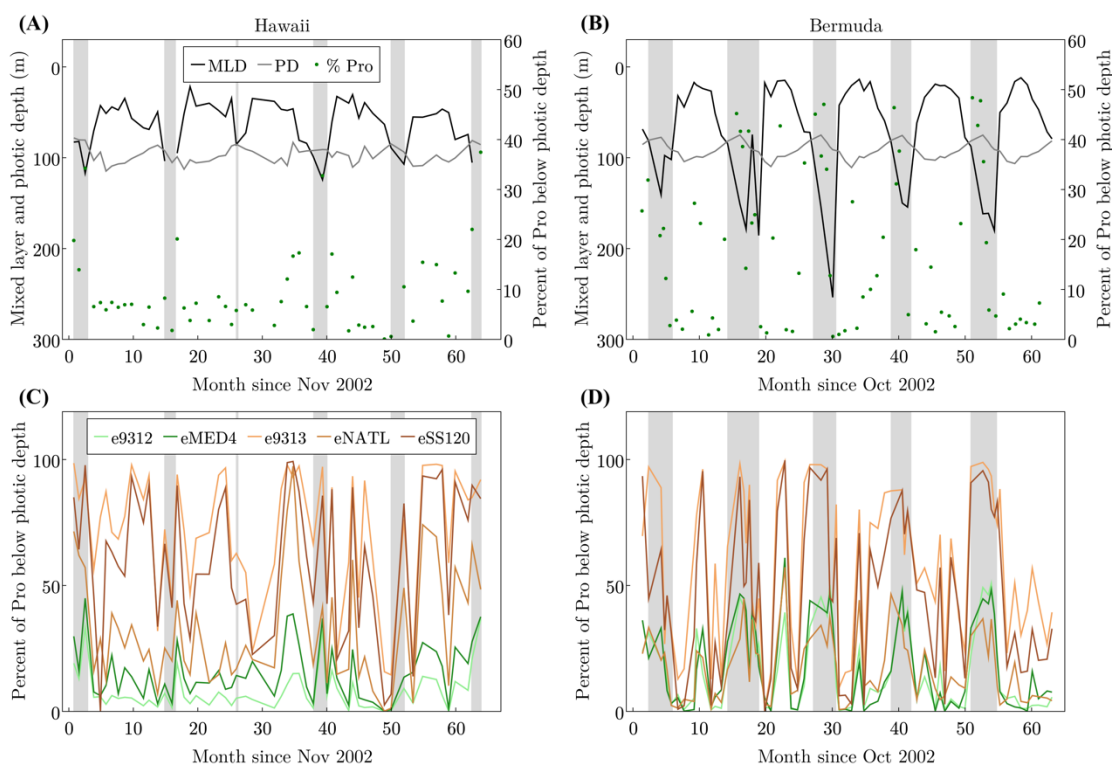
230 **Figure 3. Vertical profiles of simulated autotrophs and mixotrophs in the individual-based**  
 231 **model.** The red and blue shades in all panels indicate the differences between an ensemble of 10  
 232 model runs. (A) Vertical profiles of cell density of simulated autotrophs (blue) and mixotrophs  
 233 (red). The vertical profile of PAR is represented as the gray dashed line. (B) Vertical profiles of cell  
 234 division rate of autotrophs (blue) and mixotrophs (red). The blue and red stripes indicate the  
 235 transition point from nutrient limitation to carbon limitation of phytoplankton growth. The black  
 236 dotted line represents the contributions of DOC uptake to total carbon acquisition in mixotrophs.  
 237 (C) Vertical profiles of phosphate in simulations of autotroph (blue) and mixotroph (red).

238

239 *Interpretation of vertical distributions of Prochlorococcus ecotype at time-series stations.*

240 To what extent does mixotrophy supports natural, genetically-diverse, populations of  
 241 *Prochlorococcus*? To answer this question, we calculated the fraction of the *Prochlorococcus* cells  
 242 and of individual ecotypes living below the depth where they can be supported by photosynthesis  
 243 alone over a 5-year time series in the north Atlantic and Pacific gyres (Hawaii and Bermuda time  
 244 series study sites, respectively<sup>23</sup>). We consider only the time of the year when the water column

245 is stratified (white regions in Figure 4), defined here as a mixed layer depth that is shallower than  
246 the photic depth (light intensity is  $>10 \mu\text{mol photons m}^{-2} \text{s}^{-1}$  for high-light strains or  $> 2.8$   
247  $\mu\text{mol photons m}^{-2} \text{s}^{-1}$  for low-light strains, experimentally-determined minimal light  
248 requirement for active growth of high-light and low-light adapted strains during a 14:10 day-night  
249 cycle<sup>24</sup>). This is because at other times cells below the photic depth but still within the upper mixed  
250 layer could be transferred closer to the surface and therefore receive increased light. An average  
251 of  $\sim 8\text{-}10\%$  of the *Prochlorococcus* cells during these stratified periods are likely to be light-starved  
252 (Figure 4 A, B), including the vast majority of LL adapted ecotypes (Figure 4C, D).



253

254 **Figure 4: Estimating the number of *Prochlorococcus* cells and of specific ecotypes found below**  
255 **their photic depth at Hawaii and Bermuda.** (A), (B) The percent of total *Prochlorococcus* cells  
256 (Pro) found below their photic zone at Hawaii (A) and Bermuda (B), defined as the integrated  
257 illumination level supporting the growth of representative strains in laboratory cultures<sup>24</sup> (grey  
258 line shows this depth for HL strains). The black line shows the mixed layer depth (MLD), the grey  
259 line shows the photic depth (PD), the green dots represent the percentages of *Prochlorococcus*  
260 below photic depth, the grey areas are non-stratified conditions where cells may be mixed from

261 depth to the surface. (C), (D) The percentage of each *Prochlorococcus* ecotype below its photic  
262 depth. The data are taken from Malmstrom et al.<sup>23</sup>.

263

## 264 **Conclusions**

265 We have presented several lines of evidence illustrating the importance of mixotrophic carbon  
266 assimilation by *Prochlorococcus*. The uptake of isotopically labelled nitrogen uptake in samples  
267 from the Mediterranean Sea indicate doubling times at the DCM of about a week, consistent with  
268 cell-cycle based observations from the Equatorial and Subtropical Pacific<sup>27,29-32</sup>. The associated  
269 uptake of labelled carbon suggests that this growth rate is only viable if more than three-quarters  
270 of assimilated carbon is sourced from organic matter. Using a laboratory-calibrated model of  
271 carbon-specific photosynthesis rates and local environmental data, we compared carbon-limited  
272 growth rates with observed cell-cycle observations at the Pacific locations. We estimated that  
273 18-25% of depth integrated, net carbon assimilation by *Prochlorococcus* is heterotrophic at those  
274 sites, with as much as 80% heterotrophic carbon supply at the DCM. We note that while this shifts  
275 perception of the photo-autotrophic nature of primary producers, products such as remote-  
276 sensing based estimates of global-scale primary production are typically calibrated with data from  
277 isotopically labeled inorganic carbon studies and hence, other sources of error notwithstanding,  
278 are appropriately estimating photosynthesis and not growth rates. We explored the wider  
279 consequences of the phenomenon in simulations with an individual-based model that resolves a  
280 DOC-like substance. These simulations suggest that such extensive mixotrophy in the deeper  
281 photic layer will significantly deepen the nutricline. This is significant for carbon cycle simulations,  
282 most of which do not currently resolve mixotrophy and may predict, or inappropriately tune, a  
283 too-shallow nutricline. Finally, investigation of the ecotypic, vertical biogeography in the  
284 subtropical North Pacific and North Atlantic<sup>23</sup> indicates that low-light adapted *Prochlorococcus*  
285 spend 50-100% of their time, depending on season, below the deepest horizon for photo-  
286 autotrophically viable maintenance of the population. We propose that reliance on mixotrophy,  
287 rather than on photosynthesis, underpins the ecological success of a large fraction of the global  
288 *Prochlorococcus* population and its collective genetic diversity.

289

## 290 **Materials and Methods**

291 *Isotope labelling and phylogenetic analysis of a natural marine bacterioplankton population at sea*

292 Mediterranean seawater was collected during August 2017 (station N1200, 32.45°N, 34.37°E)  
293 from 11 depths by Niskin bottles and divided into triplicate 250 ml polycarbonate bottles. Two  
294 bottles from each depth were labeled with 1mM Sodium bicarbonate-<sup>13</sup>C and 1mM Ammonium-  
295 <sup>15</sup>N chloride (Sigma-Aldrich, USA) and all 3 bottles (2 labelled and 1 control) were incubated at the  
296 original depth and station at sea for 3.5 hours around mid-day. The short incubation time was  
297 chosen to minimize isotope dilution and potential recycling and transfer of <sup>13</sup>C and <sup>15</sup>N between  
298 community members<sup>25</sup>. After incubation, bottles were brought back on board and the incubations  
299 were stopped by fixing with 2X EM grade glutaraldehyde (2.5% final concentration) and stored at  
300 4 °C until sorting analysis. Cell sorting, NanoSIMS analyses and the calculation of uptake rates  
301 were performed as described in Roth-Rosenberg et al.<sup>26</sup>.

302

303 *DNA collection and extraction from seawater*

304 Samples for DNA were collected on 0.22 µm Sterivex filters (Millipore). Excess water was removed  
305 using a syringe, 1 ml Lysis buffer (40 mM EDTA, 50 mM Tris pH 8.3, 0.75 M sucrose) was added  
306 and both ends of the filter were closed with parafilm. Samples were kept at -80°C until extraction.  
307 DNA was extracted by using a semi-automated protocol including manual chemical cell lysis  
308 before the automated steps. The manual protocol began with thawing the samples, then the  
309 storage buffer was removed using a syringe and 170 µl lysis buffer added to the filters. 30 µl of  
310 Lysozyme (20 mg/ml) were added to the filters and incubated at 37°C for 30 min. After incubation,  
311 20 µl proteinase K and 200 µl buffer AL were added to the tube for 1 hour at 56°C (with agitation).  
312 The supernatant was transferred to a new tube and DNA was extracted using the QIAcube  
313 automated system and QIAamp DNA Mini Protocol: DNA Purification from Blood or Body Fluids  
314 (Spin Protocol, starting from step 6, at the BioRap unit, Faculty of Medicine, Technion). All DNA  
315 samples were eluted in 100 µl DNA free distilled-water.

316

317 *ITS PCR amplification*

318 PCR amplification of the ITS was carried out with specific primers for *Prochlorococcus*  
319 CS1\_16S\_1247F (5'-ACACTGACGACATGGTCTACACGTACTACAATGCTACGG) and Cs2 ITS\_Ar (5'-  
320 TACGGTAGCAGAGACTTGGTCTGGACCTCACCTTATCAGGG)<sup>21,22</sup>. The first PCR was performed in  
321 triplicate in a total volume of 25 µl containing 0.5 ng of template, 12.5 µl of MyTaq Red Mix

322 (Bioline) and 0.5  $\mu$ l of 10  $\mu$ M of each primer. The amplification conditions comprised steps at 95°C  
323 for 5 min, 28/25 (16S/ITS) cycles at 95°C for 30 sec, 50°C for 30 sec and 72°C for 1 min followed  
324 by one step of 5 min at 72°C. All PCR products were validated on a 1% agarose gel and triplicates  
325 were pooled. Subsequently, a second PCR amplification was performed to prepare libraries.  
326 These were pooled and after a quality control sequenced (2x250 paired-end reads) using an  
327 Illumina MiSeq sequencer. Library preparation and pooling were performed at the DNA Services  
328 (DNAS) facility, Research Resources Center (RRC), University of Illinois at Chicago (UIC). MiSeq  
329 sequencing was performed at the W.M. Keck Center for Comparative and Functional Genomics at  
330 the University of Illinois at Urbana-Champaign (UIUC).

331

### 332 *ITS Sequence processing*

333 Paired-end reads were analyzed using the Dada2 pipeline<sup>43</sup>. The quality of the sequences per  
334 sample was examined using the Dada2 'plotQualityProfile' command. Quality filtering was  
335 performed using the Dada2 'filterAndTrim' command with parameters for quality filtering  
336 `truncLen=c(290,260)`, `maxN=0`, `maxEE=c(2,2)`, `truncQ=2`, `rm.phix=TRUE`, `trimLeft=c(20,20)`.  
337 Following error estimation and dereplication, the Dada2 algorithm was used to correct sequences.  
338 Merging of the forward and reverse reads was done with minimum overlap of 4 bp. Detection and  
339 removal of suspected chimeras was done with command 'removeBimeraDenovo'. In total,  
340 388,417 sequences in 484 amplicon sequence variants (ASVs) were counted. The ASVs were  
341 aligned in MEGA6<sup>44</sup> and the first ~295 nucleotides, corresponding to the 16S gene, were trimmed.  
342 The ITS sequences were then classified using BLAST against a custom database of ITS sequences  
343 from cultured *Prochlorococcus* and *Synechococcus* strains as well as from uncultured HL and LL  
344 clades.

345

### 346 *Individual-based Model*

347 PlanktonIndividuals.jl (v0.1.9) was used to run the individual-based simulations. A full  
348 documentation is available at <https://juliaocean.github.io/PlanktonIndividuals.jl/dev/>. Briefly, the  
349 cells fix inorganic carbon through photosynthesis and nitrogen, phosphorus and DOC from the  
350 water column and grow until division or grazing. Cell division is modeled as a probabilistic function  
351 of cell size. Grazing is represented by a quadratic probabilistic function of cell population. Cells  
352 consume nutrient resources which are represented as Eulerian, density-based tracers. We set up

353 two separate simulations, each of them either has a population of an obligate photo-autotroph  
354 or a mixotroph which also consumes DOC. The initial conditions and parameters are the same for  
355 the two simulations except the ability of mixotrophy. The simulations were run with a time step  
356 of 1 minute for 360 simulated days to achieve a steady state. We run the two simulations for  
357 multiple times in order to get the range of the stochastic processes. The code of this configuration  
358 is available at [https://github.com/zhenwu0728/Prochlorococcus\\_Mixotrophy](https://github.com/zhenwu0728/Prochlorococcus_Mixotrophy).

359

### 360 *Evaluation of autotrophic growth rates.*

361 We evaluated the carbon-specific, daily-averaged carbon fixation rate,  $\mathbb{P}$  as a function of light  
362 intensity ( $I$ ,  $\mu E$ ) as follows:

$$363 \quad \mathbb{P} = \frac{1}{\Delta t} \int_0^{\Delta t} \frac{q_{Chl}}{q_C} P_S^{Chl} \left( 1 - e^{-\alpha_{Chl} I / P_S^{Chl}} \right) e^{-\beta_{Chl} I / P_S^{Chl}} dt .$$

364 Here, following Platt et al.<sup>45</sup>:  $P_S^{Chl}$  is an empirically constrained coefficient representing the  
365 Chlorophyll-a specific carbon fixation rate ( $mol C \cdot (mol Chl)^{-1} \cdot s^{-1}$ ) and  $\frac{q_{Chl}}{q_C}$  is the molar  
366 Chlorophyll-a to carbon ratio.  $\alpha_{Chl}$  and  $\beta_{Chl}$  are empirically determined coefficients representing  
367 the initial slope of the photosynthesis-light relationship and photo-inhibition effects at high  
368 photon fluxes, respectively. Here we impose empirically determined values for  $\alpha_{Chl}$  and  $\beta_{Chl}$  and  
369  $P_S^{Chl}$  from the published study of Moore and Chisholm<sup>24</sup>. To find the maximum estimate for  
370 *Prochlorococcus* photosynthesis at different light intensities we use photo-physiological  
371 parameters for a High-Light adapted ecotype (MIT9215), acclimated at  $70 \mu mol$  photons  $\cdot m^{-2} \cdot$   
372  $s^{-1}$  and a Low-Light adapted ecotype (MIT9211), acclimated  $9 \mu E$ .  $\Delta t = 24$  hours.  $I$  is the hourly  
373 PAR, estimated by scaling the observed noon value at each depth with a diurnal variation  
374 evaluated from astronomical formulae based on geographic location and time of year<sup>33,34</sup>. The  
375 Chlorophyll to Carbon ratio,  $\frac{q_{Chl}}{q_C}$ , is estimated as a function of growth rate and light intensity using  
376 the model of Inomura et al.<sup>46</sup> which was calibrated by laboratory data from Healey<sup>47</sup>.

377 The Chlorophyll to carbon ratio,  $\frac{q_{Chl}}{q_C}$ , can be modeled as a function of growth rate and light  
378 intensity<sup>46,48</sup>. Here we use the Inomura<sup>46</sup> model (equation 17 therein) where parameters were  
379 calibrated with laboratory data from Healey<sup>47</sup>. An initial guess of the growth rate and the

380 empirically informed light intensity are used to estimate  $\frac{q_{chl}}{q_c}$ , which is then used to evaluate the  
381 light-limited, photoautotrophic growth rate

$$382 \quad \mathbb{V}_C^{auto} = \frac{P}{q_c}$$

383 from which the Chlorophyll to carbon ratio is again updated. The light-limited growth rate is used  
384 to re-evaluate the Chlorophyll to carbon ratio. Repeating this sequence until the values converge,  
385  $\mathbb{V}_C^{auto}$  and  $\frac{q_{chl}}{q_c}$  are solved iteratively.

386 The nitrogen-specific uptake rate of fixed nitrogen ( $day^{-1}$ ) is modeled as

$$387 \quad \mathbb{V}_N = \mathbb{V}_N^{max} \frac{1}{Q_N} \frac{N}{N + K_N}$$

388 where values of the maximum uptake rate,  $\mathbb{V}_N^{max}$  and half-saturation,  $K_N$ , are determined from  
389 empirical allometric scalings<sup>35</sup>, along with a nitrogen cell quota  $Q_N$  from Bertilsson et al.<sup>37</sup> (0.77  
390  $fmol N cell^{-1}$ ).

391 The P-limited growth rate, or the phosphorus-specific uptake rate of phosphate ( $day^{-1}$ ), is  
392 modeled as

$$393 \quad \mathbb{V}_P = \mathbb{V}_P^{max} \frac{1}{Q_P} \frac{PO_4^{3-}}{PO_4^{3-} + K_P}$$

394 where values of the maximum uptake rate,  $\mathbb{V}_P^{max}$  and half-saturation,  $K_P$ , are determined from  
395 empirical allometric scalings<sup>35</sup>, along with a nitrogen cell quota  $Q_P$  from Bertilsson et al.<sup>37</sup> (0.048  
396  $fmol P cell^{-1}$ ).

397

398 Iron uptake is modeled as a linear function of cell surface area ( $SA$ ), with rate constant ( $k_{Fe}^{SA}$ )  
399 following Shaked et al.<sup>36</sup>.

$$400 \quad \mathbb{V}_{Fe} = k_{Fe}^{SA} \cdot SA \frac{1}{Q_{Fe}}$$

401 The potential light-, nitrogen-, phosphorus- and iron-limited growth rates ( $\mathbb{V}_C, \mathbb{V}_N, \mathbb{V}_P, \mathbb{V}_{Fe}$ ) were  
402 evaluated at each depth in the water column and the minimum is the local modeled photo-



403 autotrophic growth rate estimate, absent of mixotrophy (blue lines, Figure 2B, D). The the model  
404 is available at [https://github.com/zhenwu0728/Prochlorococcus\\_Mixotrophy](https://github.com/zhenwu0728/Prochlorococcus_Mixotrophy).

405

406 A significant premise of this study is that heterotrophy is providing for the shortfall in carbon  
407 under very low light conditions, but not nitrogen. It is known that *Prochlorococcus* can assimilate  
408 amino acids<sup>9</sup> and therefore the stoichiometry of the heterotrophic contribution might alter the  
409 interpretations. However, it is also known that *Prochlorococcus* can exude amino acids<sup>38</sup> which  
410 might cancel out the effects on the stoichiometry of *Prochlorococcus*.

411 For the estimates of photo-trophic growth rate from local environmental conditions (Figure 2) we  
412 employed photo-physiological parameters from laboratory cultures of *Prochlorococcus*<sup>24</sup>. For the  
413 purposes of this study, we have assumed that the photosynthetic rates predicted are Net Primary  
414 Production which means that autotrophic respiration has been accounted for in the  
415 measurement. However, the incubations in that study were of relatively short timescale (45 min),  
416 which might suggest they are perhaps more representative of Gross Primary Production. If this is  
417 the case, our estimates of photo-autotrophic would be even lower after accounting for  
418 autotrophic respiration, and thus would demand a higher contribution from heterotrophic carbon  
419 uptake. In this regard, our estimates might be considered a lower bound for organic carbon  
420 assimilation.

421

## 422 **Acknowledgements**

423 We thank the captain and crew of the R/V Mediterranean Explorer and Tom Reich, for help during  
424 the work at sea, Mike Krom and Anat Tsemel for the nutrient analyses, Maya Ofek-Lalzar for  
425 assistance with the bioinformatics analysis, Annett Grützmüller for NanoSIMS routine operation,  
426 Ioannis Tsakalakis for help with hourly PAR estimation, and John Casey for the discussion about C  
427 uptakes rates. This study was supported by grant RGP0020/2016 from the Human Frontiers  
428 Science Program (to MV, HPG and DS) and by grant number 1635070/2016532 from the NSF-BSF  
429 program in Oceanography (NSFOCE-BSF, to DS). The NanoSIMS at the Leibnitz-Institute for Baltic  
430 Sea research in Warnemuende (IOW) was funded by the German Federal Ministry of Education  
431 and Research (BMBF), grant identifier 03F0626A. MJF and WZ are grateful for support from the  
432 Simons Foundation through the Simons Collaboration on Ocean Processes and Ecology (SCOPE

433 329108 to MJF) and the Simons Collaboration for Computational BIOgeochemical Modeling of  
434 marine EcosystemS (CBIOMES 549931 to MJF).

435

#### 436 **Author contributions**

437 DA, DRR, TLK, AV, MV and DS designed experiments, DRR, DA, TLK, LZ and DS performed  
438 experiments and field analyses, DRR, DA, TLK, AV, and FE performed NanoSIMS analyses, DA, DRR,  
439 TLK, AV, LZ, FE, HPG, MV and DS analyzed experimental results. WZ, MJF, OW and DS designed  
440 and executed the growth rate simulations. WZ designed and executed the individual-based model  
441 simulations. WZ, DA, DRR, TLK, MJF and DS wrote the manuscript with contributions from all  
442 authors.

443

#### 444 **Competing interests**

445 The authors declare no competing interests.

446

#### 447 **References**

- 448 1. Falkowski, P. G. The role of phytoplankton photosynthesis in global biogeochemical  
449 cycles. *Photosynthesis Research* 1994 39:3 **39**, 235–258 (1994).
- 450 2. Stoecker, D. K., Hansen, P. J., Caron, D. A. & Mitra, A. Mixotrophy in the Marine Plankton.  
451 <http://dx.doi.org/10.1146/annurev-marine-010816-060617> **9**, 311–335 (2017).
- 452 3. Hartmann, M. *et al.* Mixotrophic basis of Atlantic oligotrophic ecosystems. *Proceedings of*  
453 *the National Academy of Sciences* **109**, 5756–5760 (2012).
- 454 4. Zubkov, M. v. & Tarran, G. A. High bacterivory by the smallest phytoplankton in the North  
455 Atlantic Ocean. *Nature* 2008 455:7210 **455**, 224–226 (2008).
- 456 5. Ward, B. A. & Follows, M. J. Marine mixotrophy increases trophic transfer efficiency,  
457 mean organism size, and vertical carbon flux. *Proceedings of the National Academy of*  
458 *Sciences* **113**, 2958–2963 (2016).
- 459 6. Repeta, D. J. Unifying chemical and biological perspectives of carbon accumulation in the  
460 environment. *Proceedings of the National Academy of Sciences of the United States of*  
461 *America* vol. 118 (2021).
- 462 7. Zakem, E. J., Cael, B. B. & Levine, N. M. A unified theory for organic matter accumulation.  
463 *Proceedings of the National Academy of Sciences of the United States of America* **118**,  
464 (2021).
- 465 8. Munoz-Marin, M. d. C. *et al.* Prochlorococcus can use the Pro1404 transporter to take up  
466 glucose at nanomolar concentrations in the Atlantic Ocean. *Proceedings of the National*  
467 *Academy of Sciences* **110**, 8597–8602 (2013).

- 468 9. Zubkov, M. v., Tarran, G. A. & Fuchs, B. M. Depth related amino acid uptake by  
469 Prochlorococcus cyanobacteria in the Southern Atlantic tropical gyre. *FEMS Microbiology*  
470 *Ecology* **50**, 153–161 (2004).
- 471 10. Muñoz-Marín, M. C. *et al.* Mixotrophy in marine picocyanobacteria: use of organic  
472 compounds by Prochlorococcus and Synechococcus. *The ISME Journal* **14**, 1065–1073  
473 (2020).
- 474 11. Biller, S. J., Berube, P. M., Lindell, D. & Chisholm, S. W. Prochlorococcus: the structure  
475 and function of collective diversity. *Nature Reviews Microbiology* **13**, 13–27 (2015).
- 476 12. Rocap, G. *et al.* Genome divergence in two Prochlorococcus ecotypes reflects oceanic  
477 niche differentiation. *Nature* **424**, 1042–1047 (2003).
- 478 13. Coe, A. *et al.* Survival of Prochlorococcus in extended darkness. *Limnology and*  
479 *Oceanography* **61**, 1375–1388 (2016).
- 480 14. Vila-Costa, M. *et al.* Dimethylsulfoniopropionate Uptake by Marine Phytoplankton.  
481 *Science* **314**, 652–654 (2006).
- 482 15. Becker, J. W., Hogle, S. L., Rosendo, K. & Chisholm, S. W. Co-culture and biogeography of  
483 Prochlorococcus and SAR11. *The ISME Journal* **13**, 1506–1519 (2019).
- 484 16. Coe, A. *et al.* Coping with darkness: The adaptive response of marine picocyanobacteria  
485 to repeated light energy deprivation. *Limnology and Oceanography* **66**, 3300–3312  
486 (2021).
- 487 17. Reich, T. *et al.* Seasonal dynamics of phytoplankton and bacterioplankton at the ultra-  
488 oligotrophic southeastern Mediterranean Sea. *bioRxiv* 2021.03.24.436734 (2021)  
489 doi:10.1101/2021.03.24.436734.
- 490 18. Campbell, L. & Vaulot, D. Photosynthetic picoplankton community structure in the  
491 subtropical North Pacific Ocean near Hawaii (station ALOHA). *Deep Sea Research Part I:*  
492 *Oceanographic Research Papers* **40**, 2043–2060 (1993).
- 493 19. Moore, L. R., Rocap, G. & Chisholm, S. W. Physiology and molecular phylogeny of  
494 coexisting Prochlorococcus ecotypes. *Nature* **393**, 464–467 (1998).
- 495 20. van den Engh, G. J. *et al.* Dynamics of Prochlorococcus and Synechococcus at Station  
496 ALOHA Revealed through Flow Cytometry and High-Resolution Vertical Sampling.  
497 *Frontiers in Marine Science* **4**, 359 (2017).
- 498 21. Thompson, A. W. *et al.* Dynamics of Prochlorococcus Diversity and Photoacclimation  
499 During Short-Term Shifts in Water Column Stratification at Station ALOHA. *Frontiers in*  
500 *Marine Science* **5**, 488 (2018).
- 501 22. Ahlgren, N. A., Perelman, J. N., Yeh, Y. & Fuhrman, J. A. Multi-year dynamics of fine-scale  
502 marine cyanobacterial populations are more strongly explained by phage interactions  
503 than abiotic, bottom-up factors. *Environmental Microbiology* **21**, 2948–2963 (2019).

- 504 23. Malmstrom, R. R. *et al.* Temporal dynamics of Prochlorococcus ecotypes in the Atlantic  
505 and pacific oceans. *ISME Journal* **4**, 1252–1264 (2010).
- 506 24. Moore, L. R. & Chisholm, S. W. Photophysiology of the marine cyanobacterium  
507 Prochlorococcus: Ecotypic differences among cultured isolates. *Limnology and*  
508 *Oceanography* **44**, 628–638 (1999).
- 509 25. Berthelot, H. *et al.* NanoSIMS single cell analyses reveal the contrasting nitrogen sources  
510 for small phytoplankton. *The ISME Journal* **13**, 651–662 (2019).
- 511 26. Roth-Rosenberg, D. *et al.* Prochlorococcus cells rely on microbial interactions rather than  
512 on chlorotic resting stages to survive long-term nutrient starvation. *mBio* **11**, 1–13  
513 (2020).
- 514 27. Goericke, R. & Welschmeyer, N. A. The marine prochlorophyte Prochlorococcus  
515 contributes significantly to phytoplankton biomass and primary production in the  
516 Sargasso Sea. *Deep Sea Research Part I: Oceanographic Research Papers* **40**, 2283–2294  
517 (1993).
- 518 28. Vaultot, D. The Cell Cycle of Phytoplankton: Coupling Cell Growth to Population Growth.  
519 *Molecular Ecology of Aquatic Microbes* 303–322 (1995) doi:10.1007/978-3-642-79923-  
520 5\_17.
- 521 29. Binder, B. J., Chisholm, S. W., Olson, R. J., Frankel, S. L. & Worden, A. Z. Dynamics of  
522 picophytoplankton, ultraphytoplankton and bacteria in the central equatorial Pacific.  
523 *Deep Sea Research Part II: Topical Studies in Oceanography* **43**, 907–931 (1996).
- 524 30. Partensky, F., Blanchot, J., Lantoine, F., Neveux, J. & Marie, D. Vertical structure of  
525 picophytoplankton at different trophic sites of the tropical northeastern Atlantic Ocean.  
526 *Deep Sea Research Part I: Oceanographic Research Papers* **43**, 1191–1213 (1996).
- 527 31. Vaultot, D., Marie, D., Olson, R. J. & Chisholm, S. W. Growth of Prochlorococcus, a  
528 photosynthetic prokaryote, in the equatorial Pacific Ocean. *Science* **268**, 1480–1482  
529 (1995).
- 530 32. Liu, H., Nolla, H. & Campbell, L. Prochlorococcus growth rate and contribution to primary  
531 production in the equatorial and subtropical North Pacific Ocean. *Aquatic Microbial*  
532 *Ecology* **12**, 39–47 (1997).
- 533 33. Murray, J., Leinen, M., Feely, R., Toggweiler, R. & Wanninkhof, R. EqPac: A Process Study  
534 in the Central Equatorial Pacific. *Oceanography* **5**, 134–142 (1992).
- 535 34. Karl, D. M. & Church, M. J. Microbial oceanography and the Hawaii Ocean Time-series  
536 programme. *Nature Reviews Microbiology* vol. 12 699–713 (2014).
- 537 35. Edwards, K. F., Thomas, M. K., Klausmeier, C. A. & Litchman, E. Allometric scaling and  
538 taxonomic variation in nutrient utilization traits and maximum growth rate of  
539 phytoplankton. *Limnology and Oceanography* **57**, 554–566 (2012).

- 540 36. Shaked, Y., Kustka, A. B. & Morel, F. M. M. A general kinetic model for iron acquisition by  
541 eukaryotic phytoplankton. *Limnology and Oceanography* **50**, 872–882 (2005).
- 542 37. Bertilsson, S., Berglund, O., Karl, D. M. & Chisholm, S. W. Elemental composition of  
543 marine Prochlorococcus and Synechococcus: Implications for the ecological  
544 stoichiometry of the sea. *Limnol. Oceanogr* **48**, 1721–1731 (2003).
- 545 38. Roth-Rosenberg, D., Aharonovich, D., Omta, A. W., Follows, M. J. & Sher, D. Dynamic  
546 macromolecular composition and high exudation rates in Prochlorococcus. *Limnology  
547 and Oceanography* **66**, 1759–1773 (2021).
- 548 39. Grossowicz, M. *et al.* Prochlorococcus in the lab and in silico: The importance of  
549 representing exudation. *Limnology and Oceanography* **62**, 818–835 (2017).
- 550 40. Wu, Z. *et al.* Modeling Photosynthesis and Exudation in Subtropical Oceans. *Global  
551 Biogeochemical Cycles* **35**, e2021GB006941 (2021).
- 552 41. Bertilsson, S., Berglund, O., Pullin, M. J. & Chisholm, S. W. Release of dissolved organic  
553 matter by Prochlorococcus. *Vie et Milieu* **55**, 225–232 (2005).
- 554 42. Liu, H., Nolla, H. & Campbell, L. Prochlorococcus growth rate and contribution to primary  
555 production in the equatorial and subtropical North Pacific Ocean. *Aquatic Microbial  
556 Ecology* **12**, 39–47 (1997).
- 557 43. Callahan, B. J. *et al.* DADA2: High-resolution sample inference from Illumina amplicon  
558 data. *Nature Methods* **13**:7 **13**, 581–583 (2016).
- 559 44. Tamura, K., Stecher, G., Peterson, D., Filipski, A. & Kumar, S. MEGA6: Molecular  
560 Evolutionary Genetics Analysis Version 6.0. *Molecular Biology and Evolution* **30**, 2725–  
561 2729 (2013).
- 562 45. Platt, T., Gallegos, C. & Harrison, W. Photoinhibition of photosynthesis in natural  
563 assemblages of marine phytoplankton. (1980).
- 564 46. Inomura, K. *et al.* A Mechanistic Model of Macromolecular Allocation, Elemental  
565 Stoichiometry, and Growth Rate in Phytoplankton. *Frontiers in Microbiology* **11**, 86  
566 (2020).
- 567 47. Healey, F. P. INTERACTING EFFECTS OF LIGHT AND NUTRIENT LIMITATION ON THE  
568 GROWTH RATE OF SYNECHOCOCCUS LINEARIS (CYANOPHYCEAE)1. *Journal of Phycology*  
569 **21**, 134–146 (1985).
- 570 48. Laws, E. A. & Bannister, T. T. Nutrient- and light-limited growth of *Thalassiosira fluviatilis*  
571 in continuous culture, with implications for phytoplankton growth in the ocean1.  
572 *Limnology and Oceanography* **25**, 457–473 (1980).

573